

Simple hyperchaotic memory system with large topological entropy*

Song Tang^a, Lijuan Chen^b, Fangyan Yang^c, Qingdu Li^{c,1}

^aSchool of Computer Science and Engineering,
Key Laboratory for Neuroinformation of Ministry of Education,
University of Electronic Science and Technology of China,
Chengdu 611731, China

^bSchool of Mathematical Sciences,
University of Electronic Science and Technology of China,
Chengdu 611731, China

^cResearch Center of Analysis and Control for Complex Systems,
Chongqing University of Posts and Telecommunications,
Chongqing 400065, China
liqd@cqupt.edu.cn

Received: November 30, 2015 / **Revised:** June 1, 2016 / **Published online:** January 19, 2017

Abstract. The memory elements have been the research hot spot for a long time. However, there is a litter works on the linear memory element. This paper presents a study of a new memory system containing a linear memory element. The study shows that the system not only has two kinds of route to hyperchaos, but also exists many kinds of coexisting attractors in the phase space. Moreover, the system can generate more complex hyperchaotic behaviors. To prove it, we find a new kind of topological horseshoes with two-directional expansions that consist of three disconnected compact sets. This new kind of horseshoes suggests that the topological entropy of the hyperchaotic attractor is larger than other hyperchaotic attractors reported before. For detailed study of the hyperchaotic invariant set, we also demonstrate a method to extract the orbits from the hyperchaotic horseshoes.

Keywords: hyperchaotic memory system, route to hyperchaos, coexisting attractors, topological entropy, orbits in the hyperchaotic horseshoes.

1 Introduction

The memory circuit element is a device with memory effect [6]. Because of the ability of storing readable information, the memory element is regarded to have potential

*This work is supported in part by National Natural Science Foundation of China (grant Nos. 61501073, 61104150) and Science Fund for Distinguished Young Scholars of Chongqing (grant No. cstc2013jcyj40001).

¹Corresponding author.

applications in many fields such as artificial intelligence, computers, neuromorphic circuits, analog circuitries.

For better understanding and applying of the memory element, an essential task for the community of nonlinear circuits and systems is to exploit all complex behaviors, including chaos. Therefore, there is growing interest on chaos in simple circuits containing memory element, especially the memristor [5], which has been successfully fabricated by HPLab in 2008 [25]. Muthuswamy et al. [16] proposed the simplest chaotic system based on the Chua memristor. Bao et al. [2] studied the phenomenon of transient chaos in smooth memristor oscillator. Using the Hewlett-Packard memristor, Buscarino et al. [4] constructed a chaotic circuit. Andrew et al. [7] constructed a modified canonical Chua's circuit by employing a memristor with cubic nonlinear characteristics and studied its hyperchaotic behavior. Recently, hyperchaos was found in some memristive systems [11, 12, 32] modified from the Lorenz system, the Chua circuit and a chaotic Hopfield neural network, respectively.

However, the existing works are all based on the nonlinear memory element. It is of equal importance to see the other memductance function. As the simplest memory element, whether the linear memory element can lead to complex phenomena or not, is an interesting problem.

Hyperchaotic systems are the ones with two or more positive Lyapunov Exponents (LE). In many engineering-oriented fields [10, 17, 23, 28], hyperchaos is often a better choice than general chaos. Therefore, researchers paid much attention on constructing novel hyperchaotic system. For example, Wang et al. [26] proposed a four-dimensional Lorenz-like hyperchaotic system by adding linear feedback. Rech et al. [20] constructed a new hyperchaotic Chua system, in which the Chua diode was replaced by a cubic polynomial. In [30], Wang et al. proposed a hyperchaotic system without equilibrium.

In this paper, we propose a new hyperchaotic memory system modified from the Qi chaotic system by adding the linear memory element. In order to investigate the dynamical behavior of the system, the bifurcation analysis [27, 29] is firstly taken. As for the evaluation of the complexity, we adopt the more reliable topological horseshoes with computer assisted research. This method not only is rigorous in mathematics, but also can be used to prove the existence of chaos, reveal the structure of chaotic attractors and uncover the mechanism behind chaotic phenomena [9, 15, 34]. In comparison, the general evaluation methods, for example LE and correlation dimension [35, 36], are often impacted by computational parameters and numerical errors. Finally, for detailed study of the hyperchaotic invariant set, we propose a method to extract the orbits from the hyperchaotic horseshoes.

The contributions of this paper lay in the following three aspects.

First, we construct a new hyperchaotic memory system using the linear memory element. The new system has three specialties, which make it different from any other hyperchaotic systems reported before: 1) this system has an infinite number of unstable equilibria; 2) there exist simultaneously two different routes to hyperchaos; 3) the system has larger topological entropy than the reported in the existing literatures.

Second, it is found out that with the increasing effect of linear memory element, there emerge many kinds of coexisting attractors, which are not reported in other literature. This

phenomenon is meaningful for the memory system. We know that the memory patterns correspond to the attractors in mathematics. The coexistence of multi-attractors implies that the linear memory element can bring the system much larger capacity of memory than we thought before.

Third, we propose a general method based on mapping to extract the orbits in the topological horseshoes. To the knowledge of us, this is the first work that implements the mapping from symbolic sequences to orbits. This method provide a practical tool for observing and studying the construction of the hyperchaotic invariant set.

The rest of this paper is organized as follows. Section 2 introduces the new hyperchaotic system. Section 3 presents the bifurcation analysis. Section 4 carries out the topological entropy computation. Section 5 gives a method to extract the orbits in the horseshoes. Section 6 draws conclusion.

2 The proposed hyperchaotic memory system

In 2006, Qi et al. [19] proposed the Qi system, which was constructed by adding a cross-product nonlinear term into the Lorenz system. It is defined as

$$\begin{aligned}\dot{x} &= a(y - x) + yz, \\ \dot{y} &= cx - y - xz, \\ \dot{z} &= xy - bz.\end{aligned}\tag{1}$$

Typically, in parameter setting $a = 35$, $b = 7$ and $c = 25$, the system is chaotic.

In this paper, for generality, we do not select the most used memristor, but adopt the more general model, namely, the linear memory element. According to [3], this kind of memory element can be defined by the following equations:

$$\dot{w}(t) = y(t), \quad h(t) = (1 + w(t))y(t).\tag{2}$$

Here $y(t)$ and $h(t)$ are input and output of a memory element, respectively; $w(t)$ is the internal state variable. Obviously, if $y(t)$ and $h(t)$ correspond to voltage and current of a two-terminal electronic element, respectively, the relations of (2) define a flux-controlled memristor with linear memductance $1 + w(t)$.

Based on the chaotic system and the linear memory element above, a system containing the linear memory element can be constructed. Its dynamical equation is presented by

$$\begin{aligned}\dot{x} &= \alpha(y - x) + yz, \\ \dot{y} &= \beta x - y - xz, \\ \dot{z} &= xy - \gamma z - kh, \\ \dot{w} &= y,\end{aligned}\tag{3}$$

where $\alpha = 47$, $\beta = 28$, $\gamma = 3$, $h = (1 + w)y$ and k is a positive system parameter that indicates the strength of the linear memory element. When taking $k = 0.5$, system (3) is in the state of hyperchaos. The corresponding attractor, Poincaré maps and power spectra are shown in Figs. 1, 2 and 3, respectively.

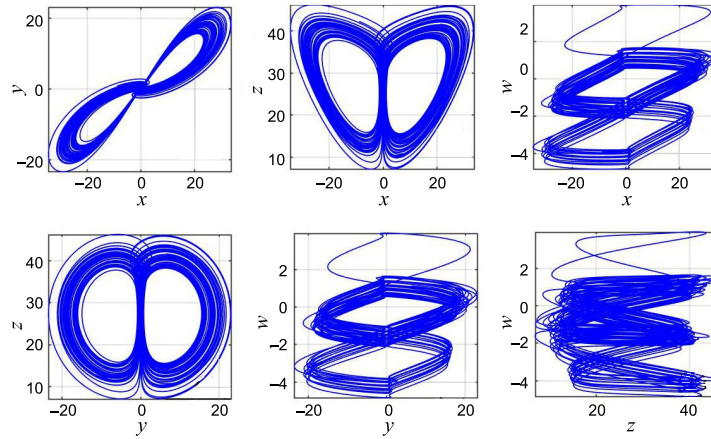


Figure 1. The projections of attractor of system (3) when $k = 0.5$.

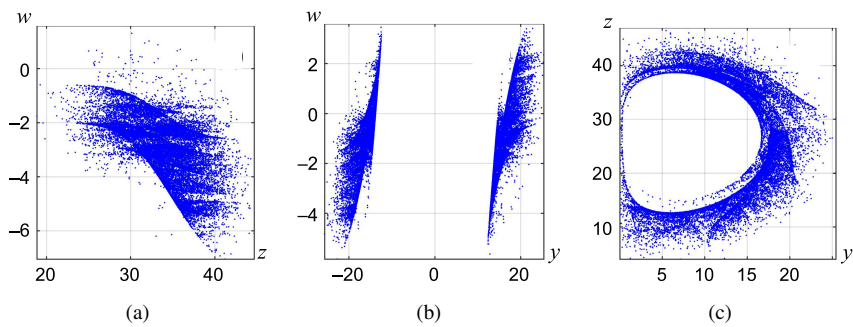


Figure 2. The Poincaré maps of system (3) when $k = 0.5$: (a) taking section $x = 0$; (b) taking section $z - 20 = 0$; (c) taking section $w = 0$.

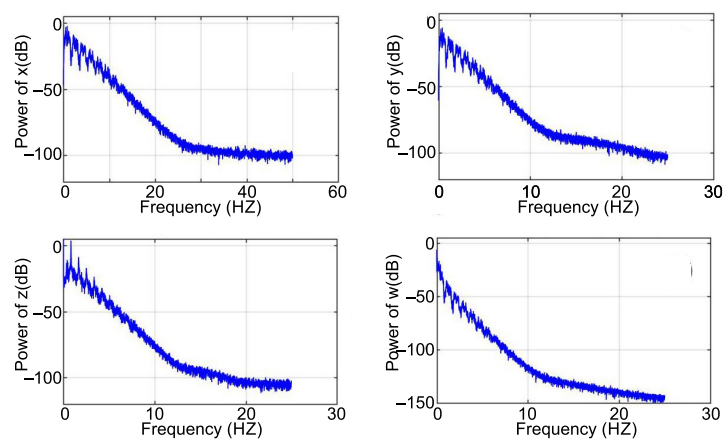


Figure 3. The power spectra of system (3).

Obviously, system (3) keeps the symmetry of the Qi system, namely, it is invariant under the transformation $(x, y, z, w) \leftrightarrow (-x, -y, z, -w)$. Since the divergence of flow $\nabla V = \partial \dot{x} / \partial x + \partial \dot{y} / \partial y + \partial \dot{z} / \partial z + \partial \dot{w} / \partial w = -53 < 0$, system (3) is dissipative and exists an attractor in its phase space.

In the following, the stability of the equilibrium points is presented. Firstly, let the right-side of Eq. (3) to be $\mathbf{0}$ and obtain

$$\begin{aligned} 47(y - x) + yz &= 0, \\ 28x - y - xz &= 0, \\ xy - 3z - k(1 + w)y &= 0, \\ y &= 0. \end{aligned}$$

By solving the algebraic equations above, it is found that the new system has infinite number of equilibrium points. We denote the equilibrium points as $O = (0, 0, 0, s)$, in which s is an arbitrary real number.

And then, by linearizing system (3), the Jacobian matrix on O is obtained:

$$J_O = \begin{pmatrix} -47 & 47 & 0 & 0 \\ 28 & -1 & 0 & 0 \\ 0 & -k(1 + s) & -3 & 0 \\ 0 & 1 & 0 & 0 \end{pmatrix}.$$

Since the eigenvalues of J_O are $\lambda_1 = -3$, $\lambda_2 = 0$, $\lambda_3 = -66.9535$, $\lambda_4 = 18.9535$, the equilibrium points of system (3) are unstable. Moreover, their stability is not related to the strength of the feedback k and the value of s .

3 Bifurcation analysis

3.1 Complex dynamical behaviors

In most works, the Lyapunov exponents are used as the indicator of systems state.

- 1) for hyperchaotic attractor, $\lambda_1 > 0$, $\lambda_2 > 0$, $\lambda_3 = 0$, $\lambda_4 < 0$;
- 2) for chaotic attractor, $\lambda_1 > 0$, $\lambda_2 = 0$, $\lambda_3 < 0$, $\lambda_4 < 0$;
- 3) for torus, $\lambda_1 = 0$, $\lambda_2 = 0$, $\lambda_3 < 0$, $\lambda_4 < 0$;
- 4) for limit cycle, $\lambda_1 = 0$, $\lambda_2 < 0$, $\lambda_3 < 0$, $\lambda_4 < 0$.

In Fig. 4, we present the spectrum of the first three LEs from initial point $x_0 = (0.1, 0, 0.1, 0)$ when $0 \leq k \leq 0.64$. From this figure it is seen that the system has complex dynamical behaviors. According to the figure, we can see clearly:

1) The hyperchaotic attractor is emerged in system (3) for $0.218 < k \leq 0.3034$, $0.325 < k \leq 0.426$ and $0.467 < k \leq 0.609$ except some isolated region. Taking $k = 0.5$, the LEs are $\lambda_1 = 0.4238$, $\lambda_2 = 0.0914$, $\lambda_3 = -5.47e - 5$, $\lambda_4 = -51.498$. For the Lyapunov dimension $D_L = 3 + (\lambda_1 + \lambda_2) / |\lambda_4| = 3.01$, system (3) is fractal. The hyperchaotic attractor is shown in Fig. 5(a).

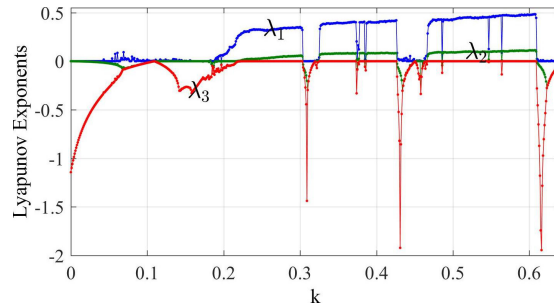


Figure 4. The first three LEs spectrum under the initial condition $x_0 = (0.1, 0, 0.1, 0)$ as k increases.

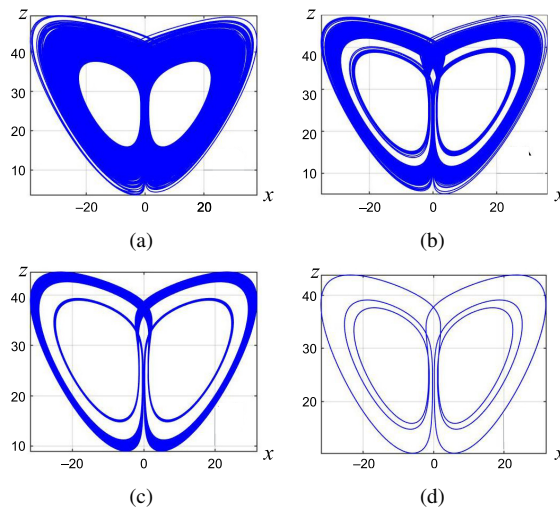


Figure 5. The attractor of system (3): (a) the hyperchaotic attractor when $k = 0.5$, (b) the chaotic attractor when $k = 0.208$, (c) the torus when $k = 0.16$, (d) the limit cycle with 3 period when $k = 0.62$.

2) The chaotic attractor is emerged in system 3 for $0.198 < k \leq 0.218$. Taking $k = 0.208$, the LEs are $\lambda_1 = 0.146$, $\lambda_2 = -2.5e - 6$, $\lambda_3 = -0.044$, $\lambda_4 = -51.09$. For the Lyapunov dimension $D_L = 3 + (\lambda_1)/|\lambda_3 + \lambda_4| = 3.0029$, system (3) is fractal. The chaotic attractor is shown in Fig. 5(b).

3) The torus is emerged in system (3) for $0.159 < k \leq 0.181$. Taking $k = 0.16$, the LEs are $\lambda_1 = 1.366e - 5$, $\lambda_2 = -3.356e - 5$, $\lambda_3 = -0.3064$, $\lambda_4 = -50.70$. The torus is shown in Fig. 5(c).

4) The limit cycle is emerged in system (3) for $0 < k \leq 0.053$, $0.304 < k \leq 0.321$ and $0.614 < k \leq 0.64$. Taking $k = 0.62$, the LEs are $\lambda_1 = 7.93e - 05$, $\lambda_2 = -0.136$, $\lambda_3 = -0.658$, $\lambda_4 = -50.2$. The limit cycle of period 3 is shown in Fig. 5(d).

5) Meanwhile, it is can be seen that the LEs are discontinuous for $0.053 < k \leq 0.159$, $0.181 < k \leq 0.198$ and $0.426 < k \leq 0.467$, which implies that there exist multi-attractor. Using the method of attraction basin, we find out that there are many kinds of coexisting

Table 1. Coexisting attractors and their initial values and Lyapunov exponents.

k	Initial condition $(x, 10, z, w)$	LE $(\lambda_1, \lambda_2, \lambda_3, \lambda_4)$	Attractor type
0.5000	$(0.1, 10, 0.1, 0)$	$(0.42, 0.09, 0, -51.5)$	Hyperchaos
	$(98.04, 10, 35.42, 0)$	$(0, 0, -0.041, -50.9)$	Torus
0.3750	$(26, 10, 41.6, 0.65)$	$(0, -0.091, -0.091, -50.8)$	Limit cycle
	$(0.5, 10, 0.5, 0.5)$	$(0.406, 0.078, 0, -51.4)$	Hyperchaos
0.4572	$(0.1, 10, 0.1, 0)$	$(0, -0.05, -0.1412, -50.8)$	Limit cycle
	$(5, 10, 5, 0)$	$(0, 0, -0.1385, -50.8)$	Torus
0.3100	$(0.1, 10, 0.1, 0)$	$(0, -0.297, -0.297, -50.4)$	Limit cycle
	$(0.5, 10, 0.5, 0.5)$	$(0, -0.297, -0.297, -50.4)$	Limit cycle
0.3250	$(0.1, 10, 0.1, 0)$	$(0, 0, -0.0768, -50.9)$	Torus
	$(-10, 10, 10, 0)$	$(0, 0, -0.058, -51.0340)$	Torus

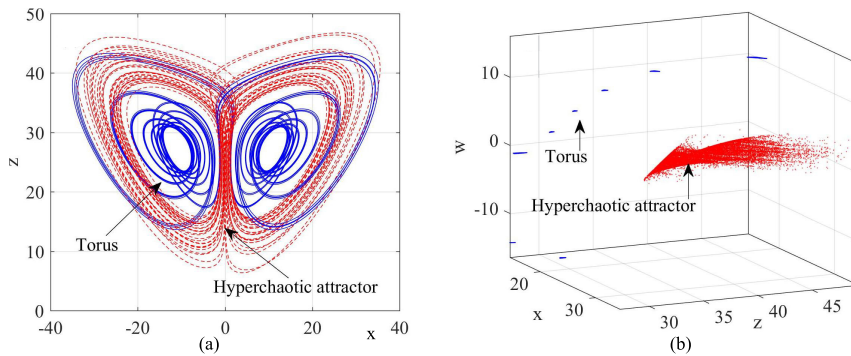


Figure 6. The coexisting hyperchaos and torus when $k = 0.5$: (a) the attractors of the system (3), (b) the attractors of Poincaré map.

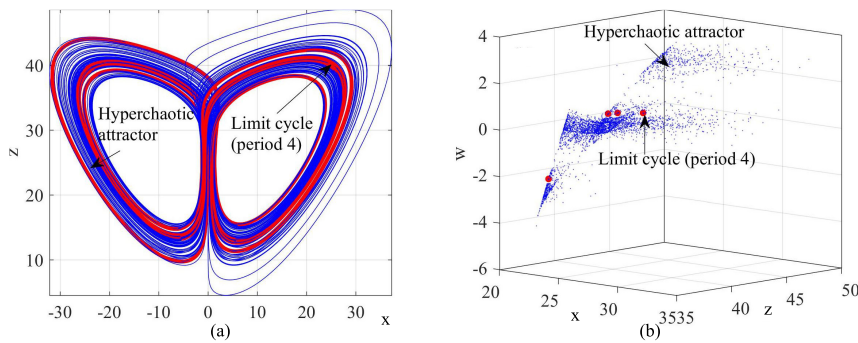


Figure 7. The coexisting limit cycle and hyperchaos when $k = 0.375$: (a) the attractors of system (3), (b) the attractors of Poincaré map.

attractors including a) coexisting hyperchaos and torus, b) coexisting limit cycle and hyperchaos, c) coexisting limit cycle and torus, d) coexisting limit cycle and limit cycle, e) coexisting torus and torus. These findings are listed in Table 1. In Figs. 6(a), 7(a), 8(a),

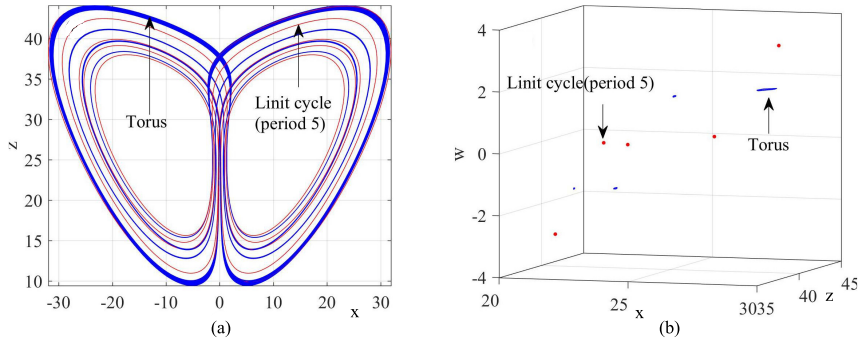


Figure 8. The coexisting limit cycle and torus when $k = 0.4572$: (a) the attractors of system (3), (b) the attractors of Poincaré map.

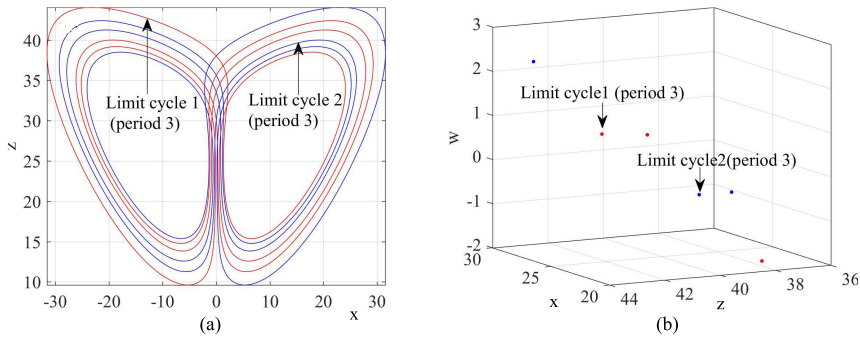


Figure 9. The coexisting limit cycle and limit cycle when $k = 0.31$: (a) the attractors of system (3), (b) the attractors of Poincaré map.

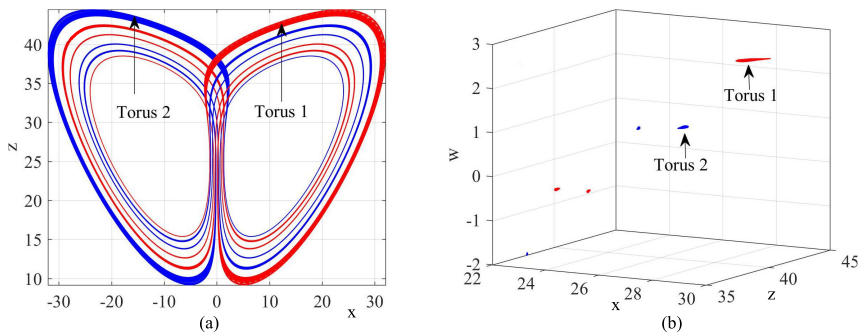


Figure 10. The coexisting torus and torus when $k = 0.325$: (a) the attractors of the system (3), (b) the attractors of Poincaré map.

9(a) and 10(a), the corresponding phase portraits are presented. Moreover, for a clear view, the attractors are also computed with the Poincaré map (taking section $y - 10 = 0$) as shown in the 3D state space in Figs. 6(b), 7(b), 8(b), 9(b) and 10(b).

3.2 The routes to hyperchaos

In order to observe the routes to hyperchaos, we draw the bifurcation diagram of system (3) when $0 \leq k \leq 0.64$ as shown in Fig. 11. In the figure, to eliminate the transient behaviors, the first 30000 points are canceled. From the figure it can be seen that the bifurcation coincides with the LEs spectrum shown in Fig. 4. Moreover, there exist two different routes to hyperchaos.

The one is the typical quasiperiod route to hyperchaos. With the increase of parameter k , system (3) goes into the three hyperchaotic regions according to same route: limit cycle, quasi periodic torus, chaos and hyperchaos in succession.

The another one is the intermittency route [8] to hyperchaos. With the decrease of parameter k , system (3) enters hyperchaos state from limit cycle directly. In order to determinate the kind of route to hyperchaos, we investigate the dynamical behavior of the system when k takes a critical value. As shown in Fig. 12, when $k = 0.3034$, the state of limit cycle and the state of hyperchaos appear alternately. The situation indicates that the system (3) goes through a transition from limit cycle to hyperchaos via an intermittency process.

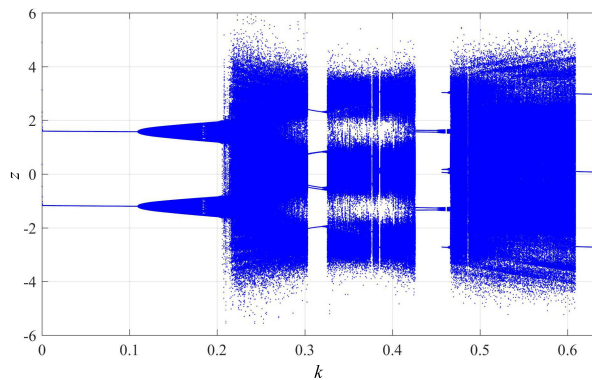


Figure 11. The bifurcation diagram of system (3) with initial condition $x_0 = (0.1, 10, 0.1, 0)$.

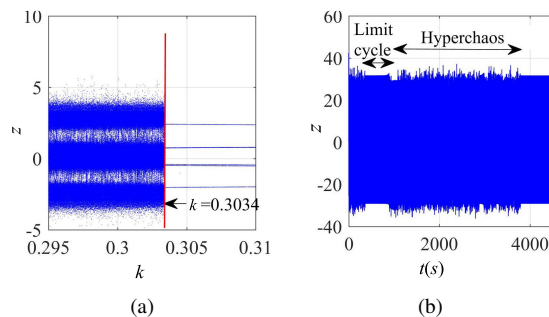


Figure 12. The intermittency route to hyperchaos of the (3): (a) the bifurcation diagram when $0.295 \leq k \leq 0.31$ ($k = 0.3034$ is the critical value of the transition from limit cycle to hyperchaos), (b) the time series of z when $k = 0.3034$.

4 Topological entropy estimation

According to the topological horseshoe theory, the topological entropy closely depends on the construction of topological horseshoe. Therefore, we arrange this section as follows: Firstly, the symbolic dynamics is introduced briefly. And then we recall the topological horseshoes theory. Finally, we detect the topological horseshoe with two-directional expanding and compute the topological entropy.

Let Σ_m be the sequence-space that consist of all bi-infinite sequences with form $s = \{\dots, s_{-n}, \dots, s_{-1}, s_0, s_1, \dots, s_n, \dots\}$, $s_i \in \{0, 1, \dots, m-1\}$.

From [31] we know that Σ_m is compact, totally disconnected and perfect. Therefore, Σ_m is a Cantor set, which frequently appears in the characterization of complex structures of chaotic invariant sets in a chaotic dynamical system.

Let $\sigma : \Sigma_m \rightarrow \Sigma_m$ to be m -shift map, it satisfies $\sigma(s_i) = s_{i+m}$.

Proposition 1. (See [31].) *The shift map σ satisfies $\sigma(\Sigma_m) = \Sigma_m$ and is continuous. As a dynamical system defined on Σ_m , σ has three properties: 1) σ has a countable infinity of periodic orbits consisting of orbits of all periods; 2) σ has an uncountable infinity of aperiodic orbits; 3) σ has a dense orbit.*

From the three conditions above it can be deduced that dynamics generated by the shift map σ is sensitive to initial conditions. Therefore, σ is chaotic.

Let X be a metric space, D be a compact subset of X and $f : D \rightarrow X$ be a map. Assuming that there exists m mutually disjoint compact subsets $\{D_i, i = 1, \dots, m\}$ of D and $f|_{D_i}$ is continuous. For each D_i , D_i^1 and D_i^2 indicate two disjoint compact subsets of D_i contained in the boundary ∂D_i .

Definition 1. (See [33].) A connected subset l of D_i is said to connect D_i^1 and D_i^2 if $l \cap D_i^1 \neq \emptyset$ and $l \cap D_i^2 \neq \emptyset$, we denote this by $D_i^1 \overset{l}{\leftrightarrow} D_i^2$. Let $\Gamma \subset D_i$ be a compact subset, Γ is said to completely separate D_i^1 and D_i^2 if for every connected subset $l \subset D_i$ with $D_i^1 \overset{l}{\leftrightarrow} D_i^2$, one has $\Gamma \cap l \neq \emptyset$, and denotes it by $\Gamma \downarrow (D_i^1, D_i^2)$.

Then the codimension-one crossing with respect to two pairs (D_i^1, D_i^2) , (D_j^1, D_j^2) is defined as following:

Definition 2. (See [13].) Let $\Gamma \subset D_i$ be a subset, we say that $f(\Gamma)$ separates D_j with respect to D_j^1 and D_j^2 if Γ contains a compact subset $\tilde{\Gamma}$ such that $f(\tilde{\Gamma}) \downarrow (D_j^1, D_j^2)$. In this case, we denote it by $f(\Gamma) \ddagger D_j$. In case that $f(\Gamma) \ddagger D_j$ holds true for every subset $\Gamma \subset D_i$ with $\Gamma \downarrow (D_i^1, D_i^2)$, we say that $f(D_i)$ separates D_j with respect to two pairs (D_i^1, D_i^2) and (D_j^1, D_j^2) , or $f(D_i) \ddagger D_j$ in case of no confusion.

Theorem 1. (See [13].) *If the codimension-one crossing relation $f(D_i) \ddagger D_j$ holds for $1 \leq i, j \leq m$, then there exists a compact invariant set $K \subset D$ such that $f|_K$ is semi-conjugate to the m -shift map, which is denoted by $\sigma|_{\Sigma_m}$.*

Since f is topologically semiconjugate to σ , which means there exists a continuous surjection $g : \Sigma_m \rightarrow X$ such that $f \circ g = g \circ \sigma$, f must be also sensitive to initial conditions, therefore, f is chaotic.

Table 2. The vertices of quadrilaterals C_1, C_2 and C_3 .

	Vertice 1	Vertice 2	Vertice 3	Vertice 4
C_1	(38.80862932, 0.67447485)	(38.63430381, 0.66910094)	(39.07360410, -0.09668142)	(39.32695718, -0.09668142)
C_2	(38.32985662, 0.62517807)	(38.30269752, 0.62517807)	(38.49610320, -0.10443726)	(38.57264247, -0.09457759)
C_3	(37.81817634, 0.70132341)	(37.79358998, 0.75909296)	(37.75232003, -0.03764536)	(37.82344484, -0.04486656)

By means of Theorem 1, we can not only rigorously proof the existence of hyperchaos, but also assess the intensity of hyperchaos by topological entropy, which can be computed by following proposition.

Proposition 2. (See [21].) *Let $f : X \rightarrow X$ be a continuous map. If there exists an invariant set $K \subset X$ such that $f|_K$ is semi-conjugate to the m -shift $\sigma|_{\Sigma_m}$, then $\text{ent}(f) \geq \text{ent}(\sigma) = \log m$. In addition, for every positive integer k , $\text{ent}(f^k) = k \cdot \text{ent}(f) \geq \log m$. Therefore, in the case, $\text{ent}(f) \geq (\log m)/k$.*

By choosing the hyperplane $\mathcal{Y} = \{(x, y, z, w) : x - 10 = 0, \dot{x} < 0\}$ as the cross-section, we obtain the Poincaré map of system (3). It is defined as: Let $\mathbf{R} : \mathcal{Y} \rightarrow \mathcal{Y}$ to be a map, for each $\mathbf{x} = (y, z, w) \in \mathcal{Y}$, $\mathbf{R}^n(\mathbf{x})$ is taken to be the n th return point in \mathcal{Y} under the flow of system (3) with the initial condition \mathbf{x} .

According to the method proposed in [11], we detect the three-dimensional horseshoes with two-directional expansions by three steps as follows.

- 1) Since that the attractor is very close to a curved surface, denoted by $y = g(z, w)$, the map \mathbf{R} can be transformed to a two-dimensional map \mathbf{P} that satisfies $\mathbf{P}(z, w) = \mathbf{R}(y = g(z, w), z, w)$.
- 2) By a serial of attempts, we find a horseshoe with two directional expansions of the map \mathbf{P} in the phase space $z \times w$. The vertices of quadrilaterals C_1, C_2 and C_3 in terms of (z, w) are listed in Table 2.
- 3) We construct the three-dimensional horseshoe of the map \mathbf{R} by projecting the planar horseshoe back to the three-dimensional space.

The final results are represented in Figs. 13, 14 and 15. To be clear, there horseshoes are shown in a new coordinate system that satisfies the relationship: $[x_1, x_2, x_3]^T = \mathbf{H}[y, z, w]^T$, where \mathbf{H} is a Householder matrix, which is expressed by

$$\mathbf{H} = \begin{bmatrix} 0.235919883300050 & -0.390152231974615 & -0.890012946281635 \\ -0.390152231974615 & 0.800781670942827 & -0.454455664908294 \\ -0.890012946281635 & -0.454455664908294 & -0.0367015542428768 \end{bmatrix}$$

Based on the three-dimensional horseshoes, we have the following theorem.

Theorem 2. *For the map \mathbf{R} , its topological entropy is $\text{ent}(\mathbf{R}) \geq (\log 3)/3$.*

Proof. From Proposition 1, to get the topological entropy of \mathbf{R} , we must proof the conclusion: for the Poincaré map \mathbf{R} , there exists a compact invariant set $A \subset (A_1 \cup A_2 \cup A_3)$, on which $\mathbf{R}^3|_A$ is semi-conjugate to the 3-shift map.

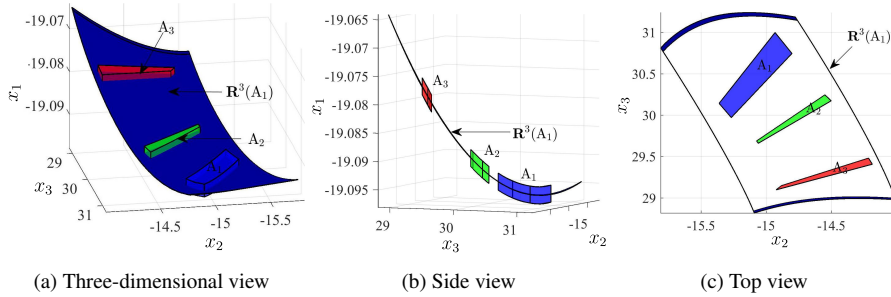


Figure 13. $R^3(A_1)$ separates $\{A_i, i = 1, 2, 3\}$.

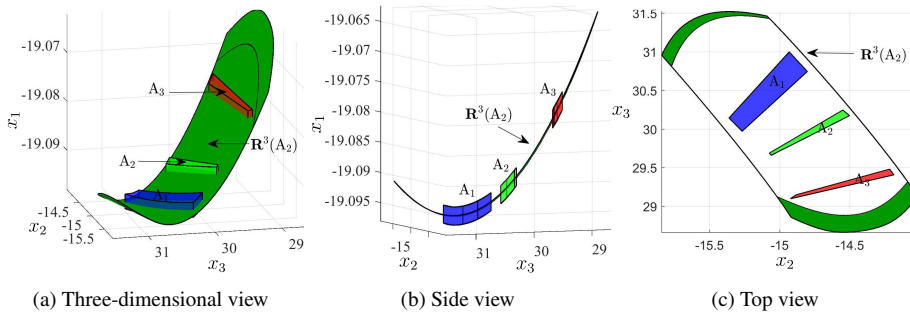


Figure 14. $R^3(A_2)$ separates $\{A_i, i = 1, 2, 3\}$.

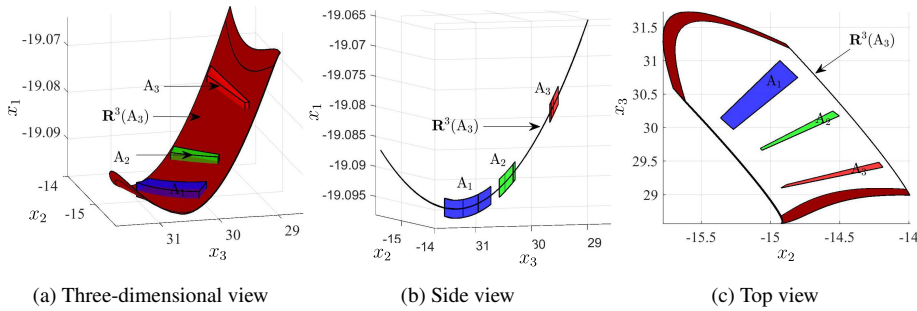


Figure 15. $R^3(A_3)$ separates $\{A_i, i = 1, 2, 3\}$.

Since that the uniqueness and continuity of solution are ensured owing to the smoothness of system (3). Therefore, we only need to show the existence of the following three relations:

- 1) $R^3(A_1) \nmid A_1, R^3(A_1) \nmid A_2, R^3(A_1) \nmid A_3;$
- 2) $R^3(A_2) \nmid A_1, R^3(A_2) \nmid A_2, R^3(A_2) \nmid A_3;$
- 3) $R^3(A_3) \nmid A_1, R^3(A_3) \nmid A_2, R^3(A_3) \nmid A_3.$

Table 3. The eigenvalues of the J_{A_1} , J_{A_2} and J_{A_3} .

	$\min \lambda_1 $	$\max \lambda_1 $	$\min \lambda_2 $	$\max \lambda_2 $
A_1	3.1780	13.307	1.516	2.306
A_2	12.957	89.665	1.143	1.517
A_3	19.905	83.993	1.124	1.741

Table 4. The topological entropy of some typical hyperchaotic systems.

System	(a)	(b)	(c)	(d)	(e)	(f)	Syst. (3)
Topol. entropy	0.0770	0.1386	0.2310	0.1733	0.3466	0.0990	0.3662

As shown in Fig. 13, under the map \mathbf{R}^3 , A_1 is compressed to $\mathbf{R}^3(A_1)$, which transversely intersects $\{A_i, i = 1, 2, 3\}$. The details show that $\mathbf{R}^3(A_1)$ across $\{A_i, i = 1, 2, 3\}$ at their middle part (see Fig.13(b)) and the four side surfaces are mapped outside $\{A_i, i = 1, 2, 3\}$ (see Fig. 13(c)). Let (A_i^t, A_i^b) be the top and bottom surface of A_i . We can have the conclusion: for each separation S of (A_i^t, A_i^b) , $f(S) \cap B_1$ must be a separation of (A_i^t, A_i^b) . Refer to Definitions 1 and 2, we have $\mathbf{R}^3(A_1) \ddagger A_1$, $\mathbf{R}^3(A_1) \ddagger A_2$, $\mathbf{R}^3(A_1) \ddagger A_3$. Analogously, from Figs. 14, 15 we can proof relations 2) and 3) mentioned above. Therefore, it is true that the codimension-one crossing relation $\mathbf{R}(D_i) \ddagger D_j$ holds for $1 \leq i, j \leq 3$.

From Theorem 1 we know that on the compact invariant set $\Lambda \subset (A_1 \cup A_2 \cup A_3)$, the map \mathbf{R}^3 is semi-conjugate to the 3-shift map. And referring to Proposition 1, we proof that the topological entropy $\text{ent}(\mathbf{R}) \geq (\log 3)/3$. \square

Additionally, since that $\mathbf{R}^3(A_i)$, $i = 1, 2, 3$, expands in two directions, the expansions along each trajectory in Λ are also in two directions. So, there must exist two positive Lyapunov exponents. Therefore, the system is hyperchaotic. Here, in order to verify that there indeed exist the two-directional expanding in the $\mathbf{R}^3(A_i)$, the eigenvalues of the Jacobian matrices J_{A_i} on A_i , $i = 1, 2, 3$, are computed. As listed in Table 3 minimums of the first two absolute eigenvalues are larger than one.

Here we list the topological entropy of some typical hyperchaotic systems in Table 4. Among them, system (a) is the Rössler [22], which is the first hyperchaotic system; system (b) is the hyperchaotic Hénon map [1] that is a typical discrete-time hyperchaotic system; system (c) is the famous Saito [24] circuit, which is a hysteresis chaos generator; system (d) is the a Lü-like hyperchaotic system [37] with an infinite number of equilibrium points; system (e) is a modified Lorenz system [18] with large LEs; system (f) is a memristive system [14], in which the introduced memristor is nonlinear. Compared with the previous systems, system (3) has the maximal topological entropy.

5 The orbits in the hyperchaotic horseshoes

It is well known that the orbits are meaningful for the study of dynamic system. From the theory of topological horseshoes we know that the horseshoes contain infinite periodic and chaotic orbits. Those orbits not only can help us to intuitively understand the behavior of

the system, but also can be applied in many applications such as the control of robot gait and the information security. In this section, we propose a simple method to extract the orbits in the new hyperchaotic horseshoes, which is obtained in Section 4.

First, the initial point is detected. Let \mathbf{F} be the three-times mapping \mathbf{R}^3 . Let \mathbf{x}_0 be the initial point. We mark the sets A_1, A_2 and A_3 with three symbols a, b and c , respectively. The given symbolic sequence with length n is defined by

$$s = \{s_1, s_2, \dots, s_i, \dots, s_{n-1}, s_n\}, \quad s_i \in \{a, b, c\}.$$

If a sequence of point satisfies the relationship as following:

$$s' = \{\mathbf{x}_0, \mathbf{x}_1, \dots, \mathbf{x}_i, \dots, \mathbf{x}_{n-1}, \mathbf{x}_n\}$$

where

$$\mathbf{x}_i = \mathbf{F}^i(\mathbf{x}_0), \quad \mathbf{x}_i \in \begin{cases} A_1, & s_i = a, \\ A_2, & s_i = b, \\ A_3, & s_i = c, \end{cases}$$

the start point of s' is the initial point \mathbf{x}_0 . In this paper, this sequence s' is called a *realization of the symbolic sequence*. Obviously, it is very hard to directly detect those points in the phase space. However, by the mapping relationship of topological horseshoes, an initial compact space, which contain the initial point \mathbf{x}_0 can be detected. In order to obtain the initial space, we construct the following sequences of sets according to the order represented by s' :

$$s'' = \{d_0, d_1, \dots, d_i, \dots, d_{n-1}, d_n\}$$

where

$$d_i \in \begin{cases} A_1, & \mathbf{x}_i \in A_1, \\ A_2, & \mathbf{x}_i \in A_2, \\ A_3, & \mathbf{x}_i \in A_3. \end{cases}$$

Then the initial space can be found by the following iteration process:

$$\begin{aligned} D_1 &= \mathbf{F}^{-1}(\mathbf{F}(d_{n-1}) \cap d_n), \\ D_2 &= \mathbf{F}^{-1}(\mathbf{F}(d_{n-2}) \cap D_1), \\ &\dots \\ D_{n-2} &= \mathbf{F}^{-1}(\mathbf{F}(d_2) \cap D_{n-3}), \\ \Omega &= \mathbf{F}^{-1}(\mathbf{F}(d_1) \cap D_{n-2}), \end{aligned}$$

where Ω is the initial space, \mathbf{F}^{-1} indicates one-time reverse mapping of \mathbf{F} . After finding the initial space, we take an arbitrary point $\mathbf{x} \in \Omega$ to be \mathbf{x}_0 . Under the initial condition, the orbit correspond to symbolic sequence s is obtained.

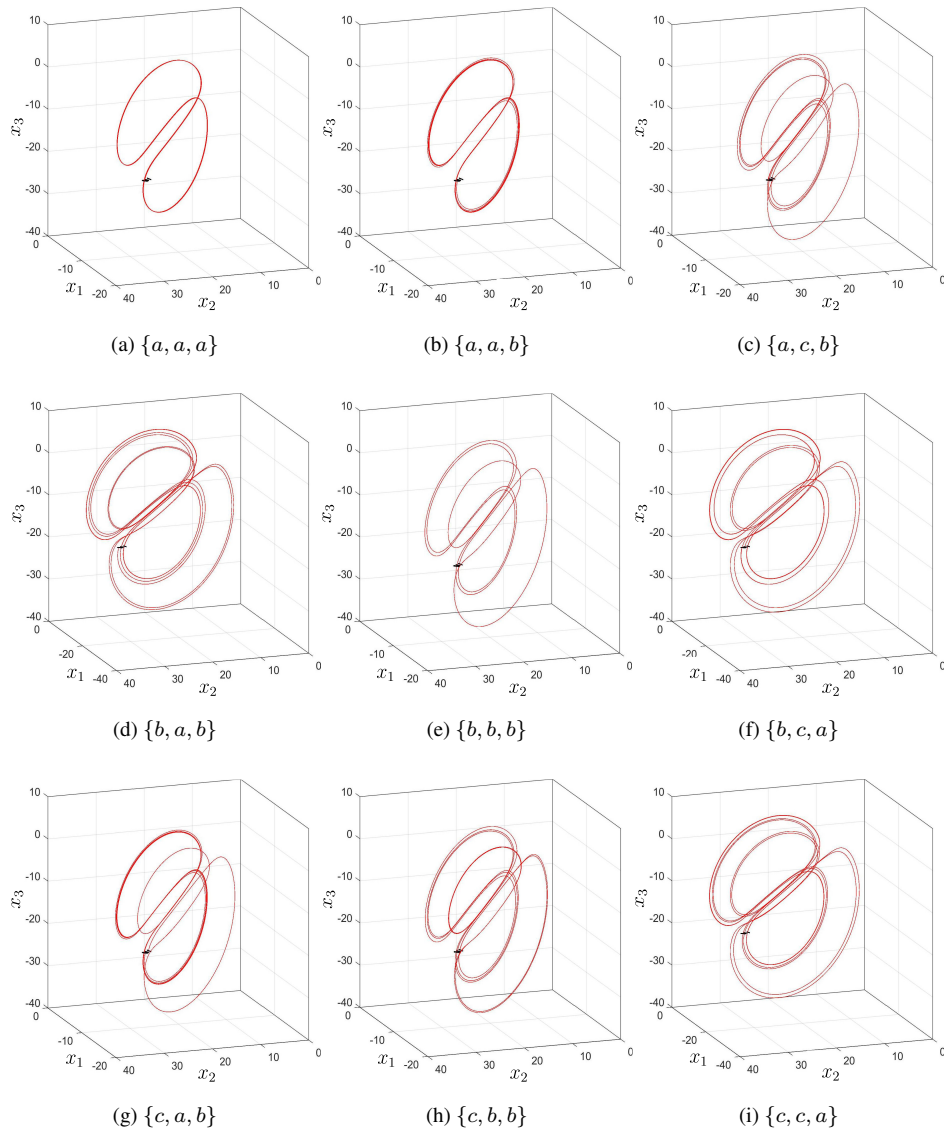


Figure 16. The orbits corresponding to some typical symbolic sequences.

In this paper, for simplicity, we only give the basic sequences, i.e. the length of sequence $n = 3$. Suppose that there is a given symbolic sequence $\{a, b, c\}$, with the method mentioned above, we get a realization, which is denoted as $\{\mathbf{x}_0, \mathbf{x}_1, \mathbf{x}_2\}$, where $\mathbf{x}_0 = [-15.0077, 30.6462, -19.0963]^T$ as shown Fig. 17(a). Correspondingly, the continuous orbit is represented in Fig. 17(b). Similarly, Fig. 16 shows the orbits corresponding to some typical symbolic sequences, and the initial points are listed in Table 5.

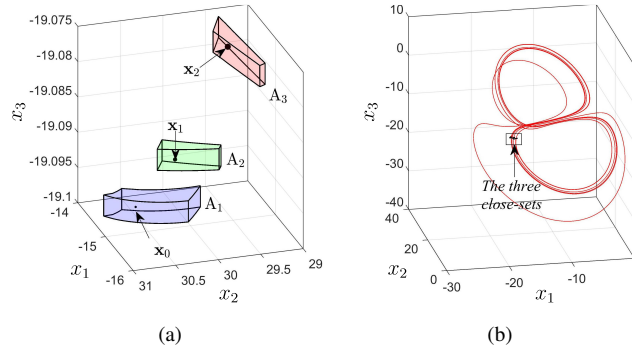


Figure 17. A realization of $\{a, b, c\}$ (a) and the corresponding orbit (b).

Table 5. The initial points of the typical symbolic sequences.

	{a,a,a}	{a,a,b}	{a,c,b}	{b,a,b}	{b,b,b}
\mathbf{x}_0	(-15.0923, 30.5918, -19.0965)	(-15.0669, 30.6412, -19.0964)	(-14.9422, 30.6065, -19.0961)	(-14.6907, 30.0665, -19.0918)	(-14.6722, 30.0849, -19.0918)
	{b,c,a}	{c,a,b}	{c,b,b}	{c,c,a}	
\mathbf{x}_0	(-14.7229, 30.0512, -19.0919)	(-14.4452, 29.3226, -19.0785)	(-14.3932, 29.3621, -19.0786)	(-14.4076, 29.3555, -19.0786)	

6 Conclusion

In this paper, we present a new four-dimensional hyperchaotic memory system, which is modified from the Qi chaotic system by introducing a simple linear memory element. For the complex dynamical behavior, we take a study in detail. By theoretical analysis, it is shown that the new system presented in this paper is symmetry, dissipative and exists an infinite number of unstable equilibrium points. The bifurcation analysis shows that the system enters the hyperchaos through two different routes and many kinds of coexisting attractors exist. In addition, in the phase space of the new system, a new kind of hyperchaotic horseshoes consisting of three compact-sets is found, by which the topological entropy is estimated.

In the end, a method is proposed to extract the orbits in the hyperchaotic horseshoes. This work provide a new view for many application. For example, in the field of chaos-based encryption, we can use the orbits in the horseshoes to modulate the information represented by the symbolic sequences. Moreover, since that the method is based on the mapping relationship, it is easy to implement by numerical method and applied directly in other kinds of horseshoes. Meanwhile, this method has some limitations. When the length of the symbolic sequences are large, the initial region of the corresponding orbits become very small owing to the fractal structure of the horseshoes. Limited to the numerical precision of the computer, it is hard to accurately express the initial region and its images. Therefore, this method is not suitable to extract the orbits for the long symbolic sequences. In future, we will pay the attentions on this problem.

Acknowledgment. We would like to thank the anonymous reviewers for their valuable comments and suggestions.

References

1. G. Baier, M. Klein, Maximum hyperchaos in generalized Hénon maps, *Phys. Lett. A*, **151**(6–7):281–284, 1990.
2. B. Bao, Z. Liu, J. Xu, Transient chaos in smooth memristor oscillator, *Chinese Phys. B*, **19**(3):030510, 2010.
3. B. Bao, X. Zou, Z. Liu, F. Hu, Generalized memory element and chaotic memory system, *Int. J. Bifurcation Chaos Appl. Sci. Eng.*, **23**(8):1350135, 2013.
4. A. Buscarino, L. Fortuna, M. Frasca, L.V. Gambuzza, A chaotic circuit based on Hewlett-Packard memristor, *Chaos*, **22**(2):023136, 2012.
5. L. O. Chua, Memristor—missing circuit element, *IEEE Trans. Circuit Theory*, **18**(5):507–519, 1971.
6. M. Di Ventra, Yu.V. Pershin, L.O. Chua, Circuit elements with memory: Memristors, memcapacitors, and meminductors, *Proc. IEEE*, **97**(10):1717–1724, 2009.
7. A.L. Fitch, D. Yu, H.H.C. Iu, V. Sreeram, Hyperchaos in a memristor-based modified canonical Chua’s circuit, *Int. J. Bifurcation Chaos Appl. Sci. Eng.*, **22**(6):1250133, 2012.
8. Q. Gao, J. Ma, Chaos and hopf bifurcation of a finance system, *Nonlinear Dyn.*, **58**(1):209–216, 2009.
9. C. Li, L. Wu, H. Li, Y. Tong, A novel chaotic system and its topological horseshoe, *Nonlinear Anal. Model. Control*, **18**(1):66–77, 2013.
10. J. Li, F. Bai, X. Di, New color image encryption algorithm based on compound chaos mapping and hyperchaotic cellular neural network, *J. Electron. Imaging*, **22**(1):013036, 2013.
11. Q. Li, S. Tang, Algorithm for finding horseshoes in three-dimensional hyperchaotic maps and its application, *Acta Phys. Sin.*, **62**(2):020510, 2013.
12. Q. Li, S. Tang, H. Zeng, T. Zhou, On hyperchaos in a small memristive neural network, *Nonlinear Dyn.*, **78**(2):1087–1099, 2014.
13. Q. Li, X. Yang, Hyperchaos from two coupled Wien-bridge oscillators, *Int. J. Circuit Theory Appl.*, **36**(1):19–29, 2008.
14. Q. Li, H. Zeng, J. Li, Hyperchaos in a 4D memristive circuit with infinitely many stable equilibria, *Nonlinear Dyn.*, **79**(4):2295–2308, 2015.
15. C. Ma, X. Wang, Hopf bifurcation and topological horseshoe of a novel finance chaotic system, *Commun. Nonlinear Sci. Numer. Simul.*, **17**(2):721–730, 2012.
16. B. Muthuswamy, L.O. Chua, Simplest chaotic circuit, *Int. J. Bifurcation Chaos Appl. Sci. Eng.*, **20**(5):1567–1580, 2010.
17. Y. Niu, X. Wang, An anonymous key agreement protocol based on chaotic maps, *Commun. Nonlinear Sci. Numer. Simul.*, **16**(4):1986–1992, 2011.
18. Y. Niu, X. Wang, M. Wang, H. Zhang, A new hyperchaotic system and its circuit implementation, *Commun. Nonlinear Sci. Numer. Simul.*, **15**(11):3518–3524, 2010.

19. G. Qi, G. Chen, S. Du, Z. Chen, Z. Yuan, Analysis of a new chaotic system, *Physica A*, **352**(2):295–308, 2005.
20. P.C. Rech, H.A. Albuquerque, A hyperchaotic Chua system, *Int. J. Bifurcation Chaos Appl. Sci. Eng.*, **19**(11):3823–3828, 2009.
21. C. Robinson, *Dynamical Systems: Stability, Symbolic Dynamics, and Chaos*, Studies in Advanced Mathematics, Vol. 28, CRC Press, Boca Raton, FL, 1999.
22. O.E. Rossler, An equation for hyperchaos, *Phys. Lett. A*, **71**(2–3):155–157, 1979.
23. D. Sadaoui, A. Boukabou, S. Hedef, Predictive feedback control and synchronization of hyperchaotic systems, *Appl. Math. Comput.*, **247**:235–243, 2014.
24. T. Saito, An approach toward higher dimensional hysteresis chaos generators, *IEEE Trans. Circuits Syst.*, **37**(3):399–409, 1990.
25. D.B. Strukov, G.S. Snider, D.R. Stewart, R.S. Williams, The missing memristor found, *Nature*, **453**(7191):80–83, 2008.
26. X. Wang, M. Wang, Hyperchaotic Lorenz system, *Acta Phys. Sin.*, **56**(9):5136–5141, 2007.
27. X. Wang, M. Wang, A hyperchaos generated from Lorenz system, *Phys. A*, **387**(14):3751–3758, 2008.
28. X. Wang, J. Zhao, An improved key agreement protocol based on chaos, *Commun. Nonlinear Sci. Numer. Simul.*, **15**(12):4052–4057, 2010.
29. X.Y. Wang, M.J. Wang, Dynamic analysis of the fractional-order Liu system and its synchronization, *Chaos*, **17**(3):113–136, 2007.
30. Z. Wang, S. Cang, E.O. Ochola, Y. Sun, A hyperchaotic system without equilibrium, *Nonlinear Dyn.*, **69**(1–2):531–537, 2012.
31. S. Wiggins, *Introduction to Applied Nonlinear Dynamical Systems and Chaos*, Texts Appl. Math., Vol. 2, Springer Verlag, New York, 2003.
32. F. Yang, J. Leng, Q. Li, The 4-dimensional hyperchaotic memristive circuit based on Chua's circuit, *Acta Phys. Sin.*, **63**(8):080502, 2014.
33. X. Yang, Computer assisted verification of chaotic dynamics, *Int. J. Bifurcation Chaos Appl. Sci. Eng.*, **19**(4):1127–1145, 2009.
34. E. Zambrano-Serrano, E. Campos-Cantón, J.M. Muñoz-Pacheco, Strange attractors generated by a fractional order switching system and its topological horseshoe, *Nonlinear Dyn.*, **83**(3):1629–1641, 2016.
35. Y.-Q. Zhang, X.-Y. Wang, A new image encryption algorithm based on non-adjacent coupled map lattices, *Appl. Soft Comput.*, **26**:10–20, 2015.
36. Y.Q. Zhang, X.Y. Wang, A symmetric image encryption algorithm based on mixed linear–nonlinear coupled map lattice, *Inf. Sci.*, **273**(8):329–351, 2014.
37. P. Zhou, F. Yang, Hyperchaos, chaos, and horseshoe in a 4D nonlinear system with an infinite number of equilibrium points, *Nonlinear Dyn.*, **76**(1):473–480, 2014.